DOI: https://doi.org/10.24425/amm.2025.154493

ZEYNEP ÖZTÜRK TAŞ^{©1*}, ALI KALKANLI^{©1}, BILGEHAN ÖGEL^{©1}

INVESTIGATION OF MICROSTRUCTURE AND HARDNESS OF TEMPERED Fe-1C-2Si (WT.%) AND Fe-1C-2Si-2Cu-1Ni (WT.%) NANOSTRUCTURED BAINITIC STEELS

In this study, the tempering behavior of two nanostructured bainitic steels of composition Fe-1C-2Si (Alloy1) and Fe-1C-2Si-2Cu-1Ni (Alloy2) is examined and compared. The alloys were homogenized, austenitized, and isothermally held at 300°C for 12 h and 24 h, respectively. Then they were tempered at 350-500°C for 30-240 min. and investigated in terms of microstructure and hardness. It was observed that Alloy2 exhibited superior thermal stability in comparison to Alloy1. Moreover, the hardness of Alloy2 increased steadily up to a peak value under the conditions where the hardness of Alloy1 decreased gradually. The secondary hardening peaks were attributed to copper precipitation, which was evidenced by TEM investigation.

Keywords: Nanobainitic steel; precipitation hardening; tempering resistance; thermal stability; transmission electron microscopy

1. Introduction

Nanostructured bainitic (NB) steels containing high amounts of C(~1 wt.%) and Si(1.5-2 wt.%) can offer ultrahigh strength (1.8-2.1GPa) [1] without compromising ductility (19-29%) [1]. The high content of Si helps to suppress carbide precipitation, while the high C content ensures a low (125-350°C) [2] transformation temperature, which is essential for a nanoscale microstructure. The microstructure of these steels is composed of consecutive layers of very thin (<100 nm [3,4]) bainitic ferrite (BF) and retained austenite (RA) films, and RA blocks which are a few microns [2,4] in size. If transformation time is insufficient, M-A(martensite-austenite) constituents may be formed from the regions of untransformed austenite upon cooling to room temperature. In this composite-like microstructure, high strength is predominantly a consequence of the high volume fraction of the nanoscale BF films, while ductility is primarily governed by the amount, morphology and degree of mechanical stability of RA, which is the softer phase [5-7].

During tempering of carbide-free bainite, the following microstructural changes take place depending on temperature and time [3]: Recovery of dislocations, decomposition of RA [3,8] films and blocks [9] into ferrite and cementite, decomposition of bainitic ferrite[10], which has a body centered tetragonal (*bct*) [8] structure, into body centered cubic (*bcc*) ferrite and cementite, coarsening of ferrite films, growth of cementite precipitates and

finally recrystallization of ferrite. The extent of these changes determines the change in strength and toughness.

In the last two decades, numerous studies [8-15] have been conducted on the tempering response of NB steels. These studies have indicated that the thermal stability of NB steels needs to be enhanced in order to broaden their industrial applications. Among the strategies [16] developed for this purpose, the key one is to improve the thermal stability of RA [11,16], which can be achieved by decreasing the driving force for cementite precipitation. For hindering cementite precipitation, the following methods have been found to be effective: addition of cementite suppressors such as Si [3,4,17] and Al [11,14], minimization of Mn content [11], and lowering of RA carbon content [11]. RA carbon content can be decreased by addition of Ni [16], which shifts the T_0 curve left, and/or V [16,18], which leads to carbide formation.

Other strategies in the literature have focused on increasing the hardness of NB steels during tempering via secondary hardening carbides [9,16] or precipitation hardening intermetallics [19,20] and Cu [20]. Ruiz-Jimenez et.al.[9] investigated the effect of secondary hardening in two NB steels (0.6C-1.7Si-1.3Mn-1.7Cr-xMo-0.5V) containing 0.2 wt.%Mo and 1 wt.% Mo. The highest hardness increase was observed as 5% (0.2Mo) and 15% (1Mo) after tempering for 1 h at ~550°C. Hulme-Smith et al. [19] pioneered the investigation of intermetallic precipitates in NB steels. They achieved a 25% increase in hardness after tempering a silicon-free NB steel with a composition of

^{*} Corresponding author: ozturk.zeynep@metu.edu.tr



 $^{^{}m I}$ MIDDLE EAST TECHNICAL UNIVERSITY, DEPARTMENT OF METALLURGICAL AND MATERIALS ENGINEERING, ANKARA, TURKEY

0.45C-13.2Ni-2.63Al-3.99Co(wt.%) at 500°C for 1h. They observed by TEM that the tempered microstructure consisted of austenite and ferrite films, fine β (Ni,Al) precipitates embedded in ferrite and large cementite precipitates at the boundaries of ferrite [19]. Krolicka et al. [20] observed that the hardness of an ultra-fine bainitic steel of composition 0.4C-0.47Mn-7.9Ni-0.77Cu-2.80Al(wt.%) increased by ~30% after tempering at 550°C for 1 h. They explained this result by the precipitation of β (Ni,Al) and Cu.

Despite the extensive literature [21-34] on the effect of copper in many types of alloys, no research has yet been conducted by alloying high carbon NB steels with copper at a high content (>1 wt.%). In this study, the tempering response of a high carbon NB steel both with (Alloy2) and without (Alloy1) the addition of 2 wt.% Cu and 1 wt.% Ni is investigated in terms of changes in microstructure and hardness. In addition, the alloys are compared based on their thermal stability levels. Furthermore, the aging characteristics of Alloy2 are determined.

2. Materials and methods

The heats were prepared by melting in a laboratory-scale induction furnace and cast in a steel mold by open die casting. Chemical compositions of the alloys and the Ms temperatures calculated by JMatPro® are given in TABLE 1. The ingot $(260 \times 55 \times 20 \text{ mm})$ was homogenized at 1100 °C for 1h in a muffle furnace. The samples in 20×20×20 mm dimensions were used for heat treatment experiments. The samples were austenitized at 950°C for 30 min. Then some of the samples were oil quenched, while the others were transferred to a salt bath at 300°C, which is the preferred temperature for the completion of bainitic transformation within a reasonable time period. In the salt bath, Alloy1 and Alloy2 were treated for 12 h and 24 h, respectively, and then air cooled. Isothermal holding periods were determined so as to guarantee the completion of transformation according to TTT diagrams (Fig. 1) calculated with JmatPro®. The as-quenched (SQ) samples of Alloy2 and all the austempered (AT) samples were subjected to a series of tempering experiments at a temperature interval of 350°C-500°C. The tempering time varied

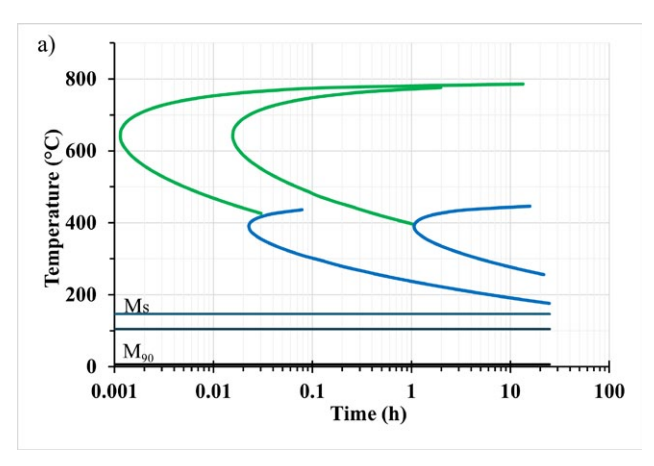


Fig. 1. TTT diagram of (a) Alloy1 (b) Alloy2

between 30 min and 240 min, in order to analyze the tempering response of the alloys.

In Alloy2, Cu and Ni were added for the purposes of precipitation hardening and prevention of hot shortness [35], respectively. In both alloys, Cr was included to provide sufficient hardenability, and Mn content was minimized to accelerate the bainitic reaction [36].

TABLE 1 Chemical composition (wt.%) and *Ms* temperature of the alloys

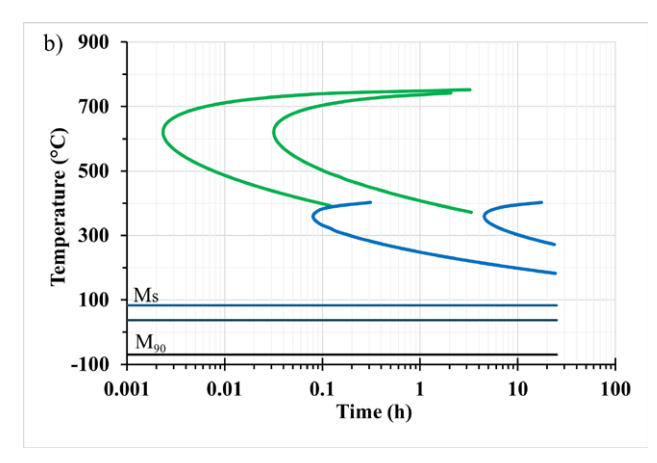
Name	C	Si	Cr	Mn	P	S	Cu	Ni	Ms (°C)
Alloy1	0.92	1.98	0.51	0.44	< 0.01	0.02	0.04	0.04	145.1
Alloy2	0.99	2.05	0.51	0.43	0.01	0.016	2.07	1.00	82.8

Samples for optical microscopy (Huvitz HDS-5800) and scanning electron microscopy (FEI 430 Nova NanoSEM and HITACHI SU5000 FE-SEM) were prepared by standard metallographic procedure and 2% nital etching. For transmission electron microscopy (JEOL JEM 2100 HRTEM), ~100 μm thick samples were electropolished (Struers-Tenupol-5 Double Jet Electropolisher) using a solution of 20% perchloric acid and 80% ethanol at $-30^{\circ}C$. Then they were ion milled (Gatan 691 Precision Ion Polishing System) at 4 kV for 1 h and 2 kV for 2 h, respectively. X-ray diffraction (Bruker D8 Advance) experiments were carried out on samples prepared in accordance with ASTM E975-13 under CuK α radiation in the 20° range of 30° -120° at a scanning speed of 1 °/min. Rietveld analysis was performed using Profex5.3 software. Five hardness measurements (Shimadzu HSV-20) per sample were made with a load of 10 kgf.

3. Results and discussion

3.1. As-quenched (SQ) and Austempered (AT) Samples

Optical micrographs of the SQ and AT samples and SEM images of AT samples are given in Figs. 2 and 3, respectively. Figs. 2-3 show that the microstructure of the SQ samples consists of martensite plates and RA blocks, while that of the AT



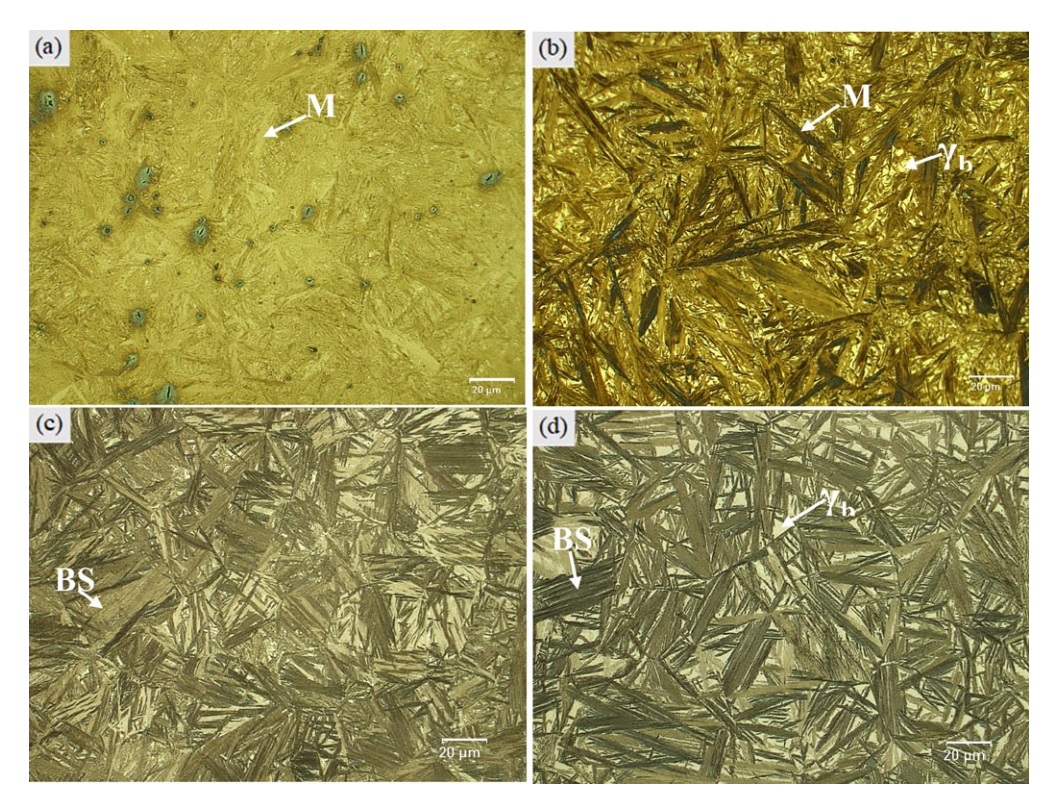


Fig. 2. Optical micrographs of as-quenched (a,b) and austempered (c,d) Alloy1 and Alloy2, respectively. White regions between martensite plates in (a,b) and bainite packages in (c,d) are RA blocks. M: Martensite, γ_b : Blocky RA, BS: Bainite sheaves

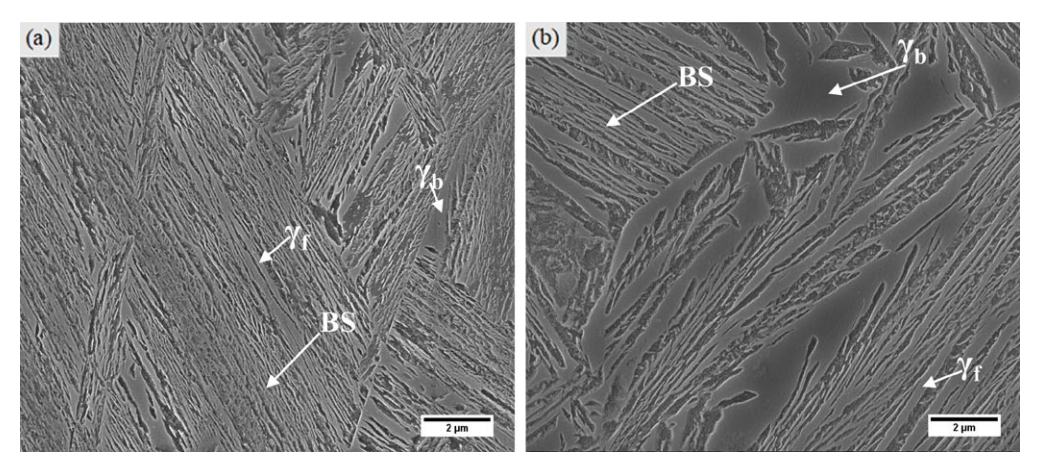


Fig. 3. SEM images of the austempered (a) Alloy1 and (b) Alloy2

samples consists of bainite packages and RA blocks. Inside the bainite packages, there exist bainitic ferrite sheaves, which are formed by consecutive layers of very thin bainitic ferrite and RA films. In both SQ and AT samples, the amount of RA in Alloy2 is higher than that in Alloy1.

The volume percentages of RA calculated from the XRD data (section 3.2.3), and the hardness values are given in TABLE 2. For both alloys, the SQ sample yields a higher hardness value than the AT sample. This is because the martensite in the SQ sample has a higher carbon content than the BF in the AT sample, and the amount of RA in the SQ sample is less than that in the AT sample. On the other hand, in both the SQ and AT conditions, Alloy2 yields a lower hardness value than Alloy1. This is due to its higher RA content, (Figs. 2-3, TABLE 2) which

results from the presence of two powerful austenite stabilizers (Cu and Ni). The Cu and Ni in Alloy2, leads to a lower Ms temperature (TABLE 1), and a T_0 curve (Fig. 4) located at lower carbon values compared to Alloy1. T_0 curve depicts, for a given

TABLE 2
RA content and hardness values of the alloys in as-quenched and austempered conditions

State	Alloy name	Hardness (HV)	Retained Austenite (vol.%)
60	Alloy1	830 ± 20	13 ± 1
SQ	Alloy2	720 ± 20	19 ± 1
AT	Alloy1	530 ± 14	21 ± 1
AI	Alloy2	445 ± 5	40 ± 2

carbon content, the temperature at which free energies of austenite and ferrite are the same. From the T_0 curve, the RA content can be estimated using Eq. (1) [37]:

$$V_{RA} = \frac{\overline{x} - x_{\alpha}}{x_{T0} - x_{\alpha}} \tag{1}$$

where \bar{x} is the average carbon content of the steel, x_{α} is the final carbon content of ferrite, which can be as high as 0.2 wt.% [9] due to the tetragonality of bainitic ferrite, and x_{T0} is the final carbon content of austenite.

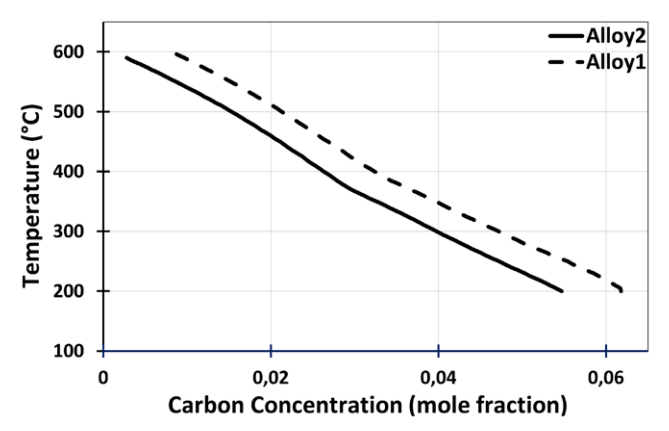


Fig. 4. T_0 curves of the alloys, which are calculated using mucg83 [38] software accounting for 400 J/mol of stored energy in ferrite due to bainitic transformation

3.2. Characterization of tempered samples

3.2.1. Retained austenite

The change in the RA content of the AT alloys after tempering at 350°C-500°C for 30-240 min is given in Fig. 5. As seen in Fig. 5, the RA content of both alloys is almost constant

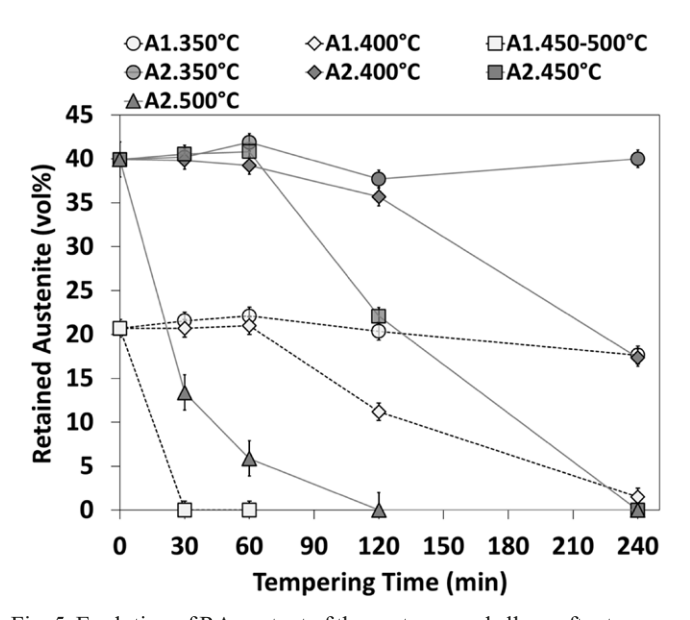


Fig. 5. Evolution of RA content of the austempered alloys after tempering at 350-500 $^{\circ}\mathrm{C}$

during tempering at 350°C for 240 min and 400°C for 60 min. However, after 120 min and 240 min at 400°C, the RA content of Alloy1 decreases by ~46% and ~93%, while that of Alloy2 decreases by only ~10% and ~56%, respectively. At 450-500°C, there is no RA left in Alloy1 after 30 min. However, even after 120 min at 450°C and 60 min at 500°C, ~45% and ~15% of the RA, respectively, is still present in Alloy2. These results will be evaluated in section 3.3, taking into account the possibility of martensite formation on cooling to room temperature.

3.2.2. Hardness

The change in hardness of the AT samples of Alloy1 and Alloy2 after tempering at 350°C-500°C for 30-240 min is given in Fig. 6 and Fig. 7, respectively.

Fig. 6 shows that during tempering at 350°C for 240 min and 400°C for 60 min, the hardness of Alloy1 remains almost constant. At 450°C, tempering causes a steady reduction in hardness in the time range of 0-240 min. This trend can be attributed to the progressive disintegration of the nanobainitic microstruc-

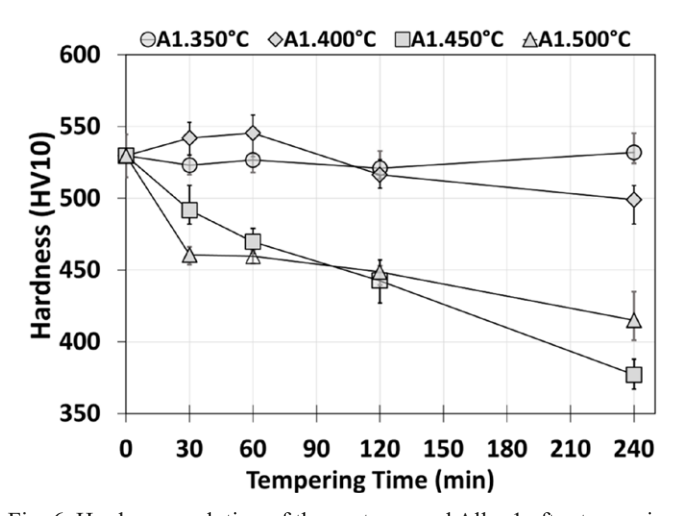


Fig. 6. Hardness evolution of the austempered Alloy1 after tempering at 350-500 $^{\circ}\mathrm{C}$

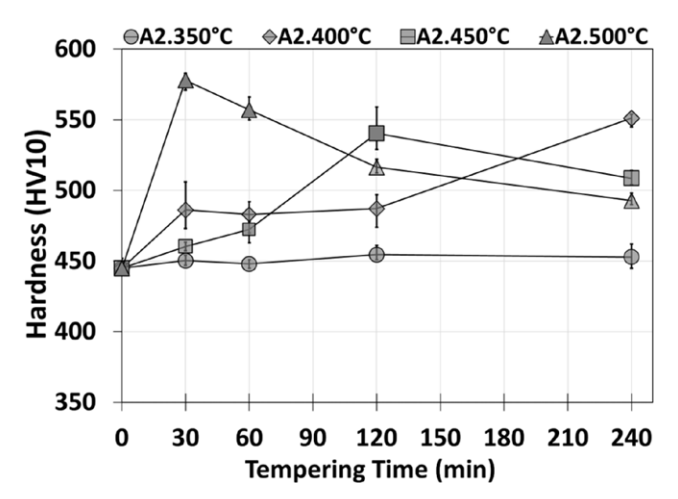


Fig. 7. Hardness evolution of the austempered Alloy2 after tempering at $350\text{-}500^{\circ}\mathrm{C}$

ture, which is mainly evidenced by the gradual decomposition of RA. (Fig. 5) At 500°C in the range of 30-240 min, the decrease in hardness is slower than at 450°C. This might be due to one or more of the following: enrichment of cementite with Cr [39], formation of alloy carbides, and formation of martensite (sec. 3.2.4) on cooling to room temperature.

On the other hand, the hardness of Alloy2 is nearly constant during tempering at 350°C for 240 min and at 400°C for 120 min. Peaks are observed at hardness values of 551HV, 540HV and 578 HV when Alloy2 is tempered at 400°C for 240 min, 450°C for 120 min and 500°C for 30 min respectively. These peaks indicate that secondary hardening becomes effective and overrides the softening caused by microstructural degradation. This secondary hardening can be ascribed to Cu precipitation since the composition of Alloy1 and Alloy2 is identical except for Cu and Ni. The effect on hardness of the possible formation of martensite on cooling to room temperature will be discussed in section 3.4.

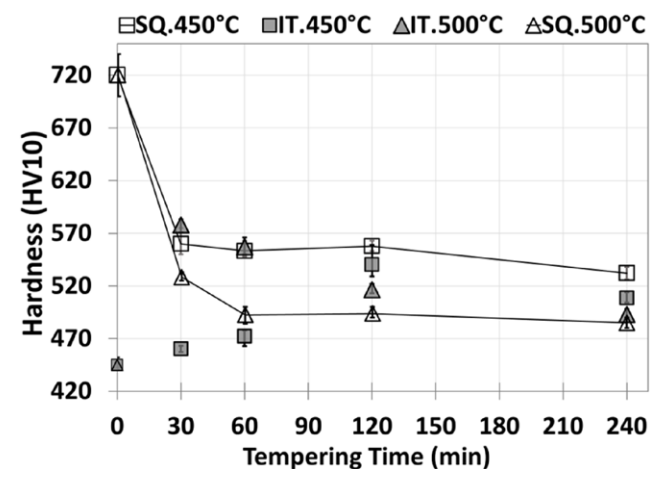


Fig. 8. Comparison of hardness evolution in as-quenched and austempered samples of Alloy2 tempered at 450°C and 500°C

Fig. 8 gives a comparison of the change in hardness of the SQ and AT samples of Alloy2 after tempering at 450° C and 500° C for 30-240 min. In the SQ samples, a sudden decrease in hardness is observed after tempering at either 450° C or 500° C for only 30 min. In the range of 60-240 min, the hardness of the SQ samples is not significantly changed by tempering. The tempered hardness values of both SQ and AT samples scatter within the same $\sim\!60$ HV band in the range of 120-240 min. It can be seen that after tempering at 500° C for 30-120 min, the AT samples yield higher hardness values than the SQ samples. The most possible reason is the formation of fresh martensite in the AT samples upon cooling to room temperature, which will be investigated in more detail in section 3.2.4.

3.2.3. XRD Patterns

XRD patterns of tempered and untempered samples of AT alloys are given in Figs. 9-12. In these figures, $2\theta^{\circ}$ interval

is chosen such that the most intense peaks of austenite and cementite can be clearly observed. The most intense peak of ferrite is included in the figure in a separate box.

Alloy1

In Fig. 9, it is shown that the ferrite peaks shift to higher $2\theta^{\circ}$ positions as tempering proceeds. This shift can be explained by the increase in the amount of *bcc* ferrite relative to *bct* ferrite due to the decomposition of bainitic ferrite (*bct* [8]) and RA into ferrite (*bcc*) and cementite. The *bcc* ferrite peaks (110, 200 and 211) are at higher $2\theta^{\circ}$ positions (Eq. (2)) (Fig. 10) than the most intense (101, 002 and 112) peaks of *bct* ferrite, respectively, due to the lower carbon content of *bcc* ferrite, which results in smaller interplanar spacings of the given diffraction planes of *bcc* ferrite with respect to those of *bct* ferrite.

$$n\lambda = 2d_{hkl}\sin\theta\tag{2}$$

where n, λ , d_{hkl} and θ denote order of diffraction, x-ray wavelength, interplanar spacing of (hkl) planes and incident angle, respectively.

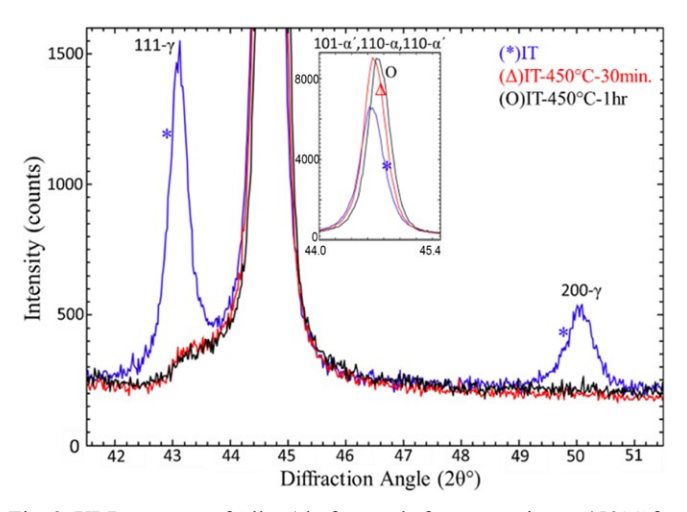


Fig. 9. XRD patterns of Alloy1 before and after tempering at 450°C for 30-60 min. α : bcc ferrite, α' : bct ferrite, γ -Fe: austenite

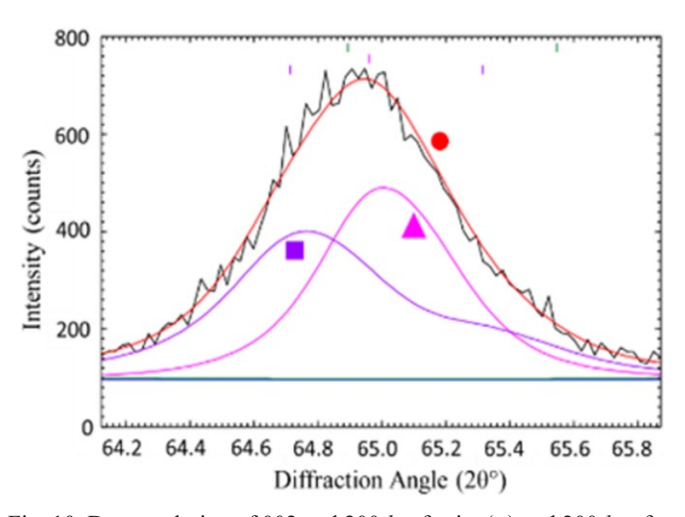


Fig. 10. Deconvolution of 002 and 200 *bct* ferrite (■) and 200 *bcc* ferrite (▲) peaks by Rietveld refinement of the XRD pattern of Alloy1 tempered at 450°C for 30 min. (•): Calculated intensity

Alloy2

In Figs. 11-12, it is shown that each RA peak, which is a convolution of thin film and blocky RA peaks, shifts significantly to a higher $2\theta^{\circ}$ angle (Eq. (2)) due to the loss of carbon [14], which reduces the interplanar spacing of the diffraction planes. At 450°C up to 60 min, the loss of carbon from RA possibly occurs via precipitation of cementite in RA [9], considering that all RA have survived as given in Fig. 5. At longer periods, the average carbon content of RA decreases mainly due to the gradual decomposition of RA starting from the films, which have a higher carbon content [3] than the RA blocks.

In Figs. 11-12, it is also shown that at 450°C and 500°C for tempering durations up to 60 min and 30 min, respectively, the ferrite peaks shift towards right due to the carbon loss from ferrite as explained above. However, the direction of the shift is reversed for the peaks of tempering at 450°C and 500°C for 120 min and 60 min, respectively. This might be explained by the partitioning of Cr and Mn between ferrite and cementite [14,39] and/or the formation of martensite (sec. 3.2.4) from the RA blocks of sufficiently low carbon content on cooling to room temperature.

For both alloys, ferrite peaks of the tempered states are narrower than those of the untempered state (Figs. 9, 11-12), which is a consequence of decreasing dislocation density, increasing crystallite size and the loss of tetragonality upon tempering [40,41].

3.2.4. Microstructure

Scanning Electron Microscopy (SEM)

SEM images of the tempered states of the AT alloys are given in Fig. 13 (Alloy1) and Figs. 15-16 (Alloy2). In Fig. 13a it is shown that the decomposition of RA films and blocks in Alloy1 is almost completed in 30 min at 450°C. When the tempering duration is increased to 60 min, further degradation of the microstructure is observed (Fig. 13b). Tempering at 500°C results in a coarser microstructure composed of ferrite and car-

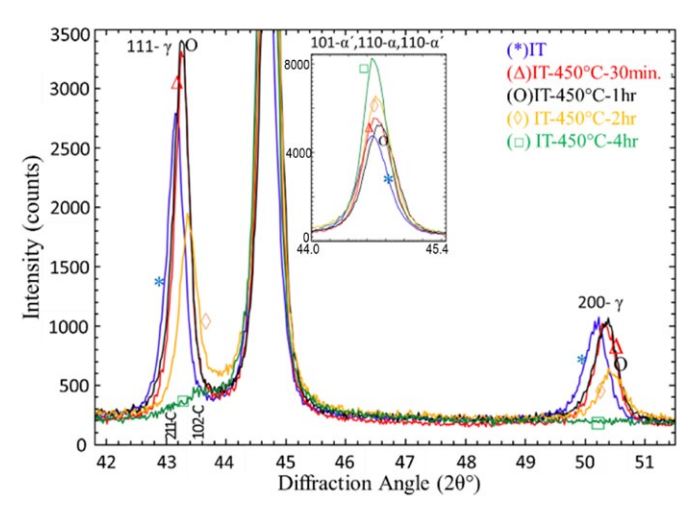


Fig. 11. XRD patterns of the austempered Alloy2 before and after tempering at 450°C for 30 min-240 min

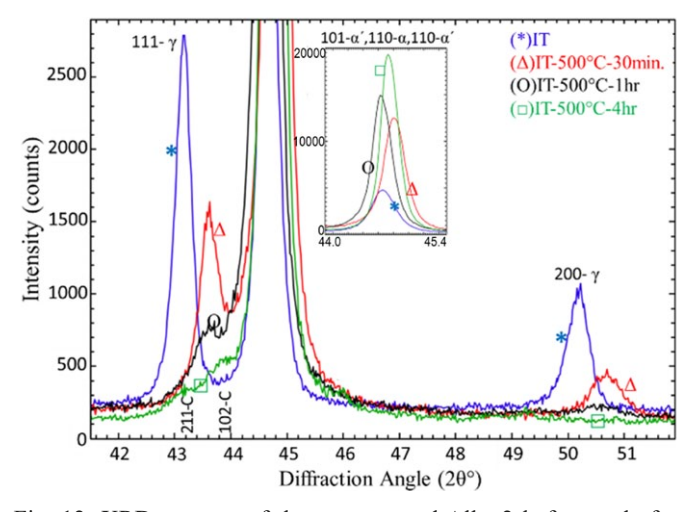


Fig. 12. XRD patterns of the austempered Alloy2 before and after tempering at 500°C for 30 min-240 min

bides (Fig. 14). It is notable that no direct evidence of martensite is observed in both Fig. 13 and Fig. 14.

In contrast to Alloy 1, Alloy 2 exhibits no microstructural changes even after 60 min of tempering at 450°C (Fig. 15a,b).

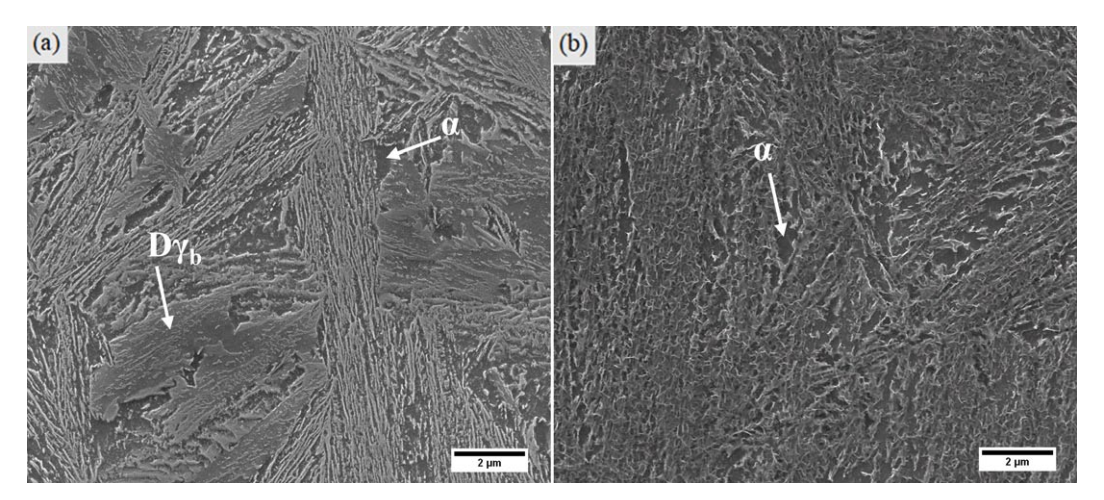


Fig. 13. SEM images of the austempered Alloy1 after tempering at 450°C for (a) 30 min and (b) 60 min. α : ferrite, $D\gamma_b$: decomposed blocky RA

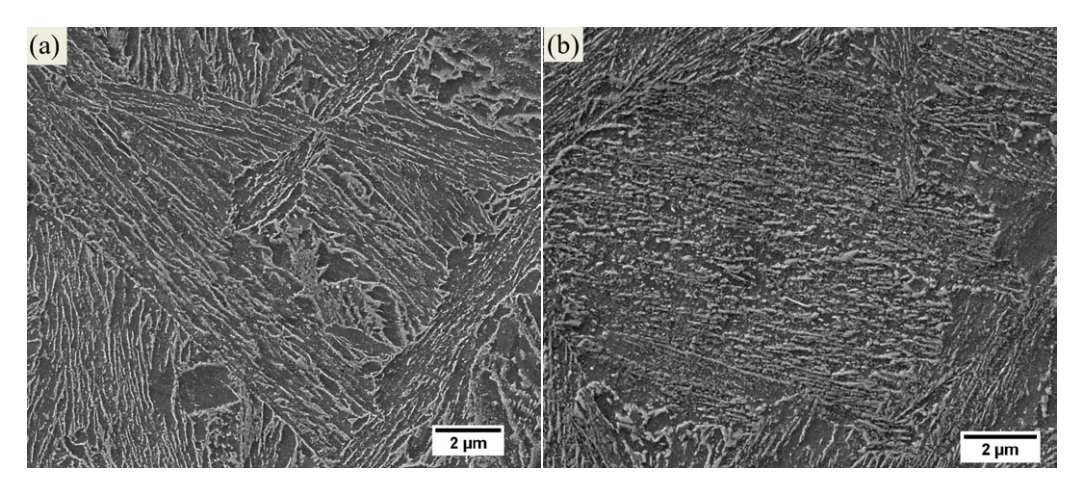


Fig. 14. SEM images of the austempered Alloy1 after tempering at 500°C for (a) 60 min and (b) 120 min

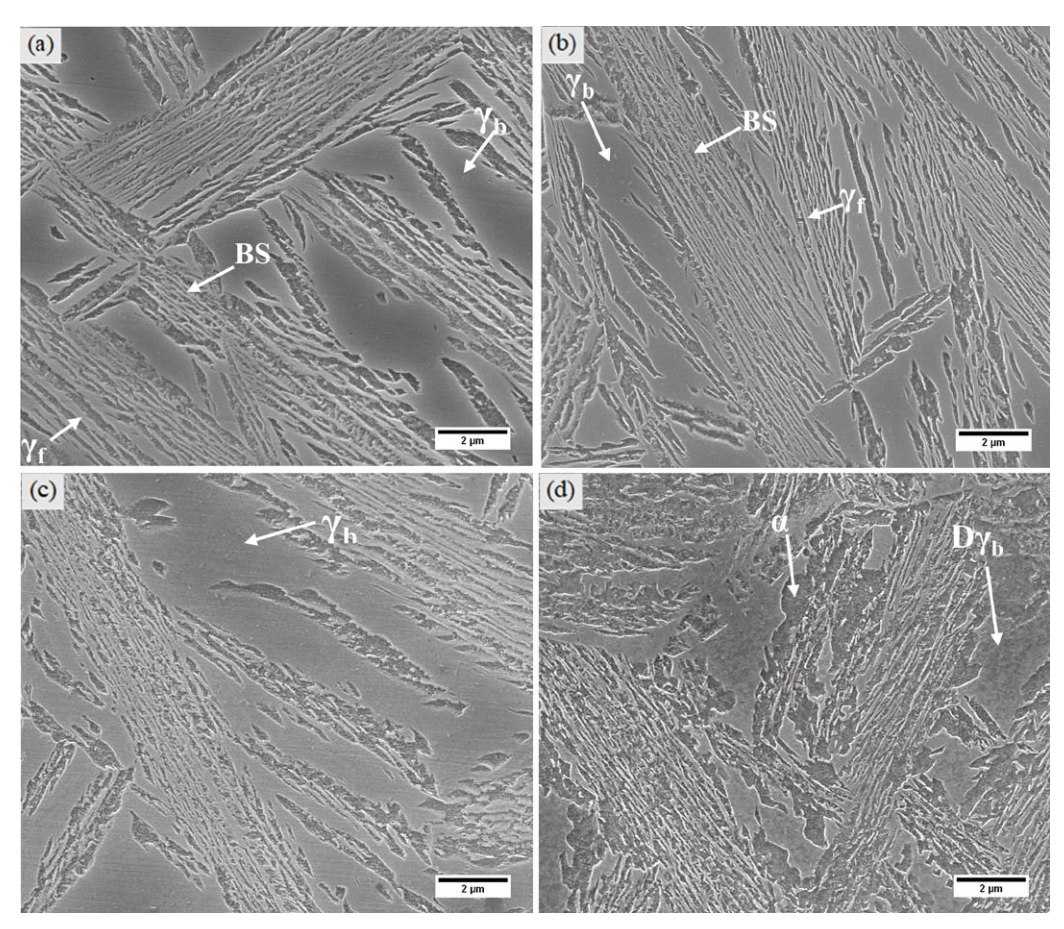


Fig. 15. SEM images of the austempered Alloy2 after tempering at 450°C for (a) 30 min, (b) 60 min, (c) 120 min, (d) 240 min. γ_b : blocky RA, $D\gamma_b$: Decomposed blocky RA, BS: Bainite sheaves

However, tempering for 120 min results in the decomposition of RA films (Fig. 15c). When the duration is increased to 240 min, RA blocks are also decomposed (Fig. 15d). At 500°C after 30 min, most of the RA films decompose and RA blocks transform into a mixture of martensite and austenite upon cooling to room temperature (Figs. 16,17). As the tempering time increases, the microstructural degradation progresses, and the amount of M-A constituents decreases (Fig. 16b,c). Finally, all RA films and blocks decompose after tempering for 240 min (Fig. 16d).

Transmission Electron Microscopy (TEM)

Two samples of Alloy2 were investigated by TEM analysis: The peak hardness sample (Fig. 18), which was tempered at 450°C for 2 h, and the overaged sample (Fig. 19) which was tempered at 500°C for 4h.

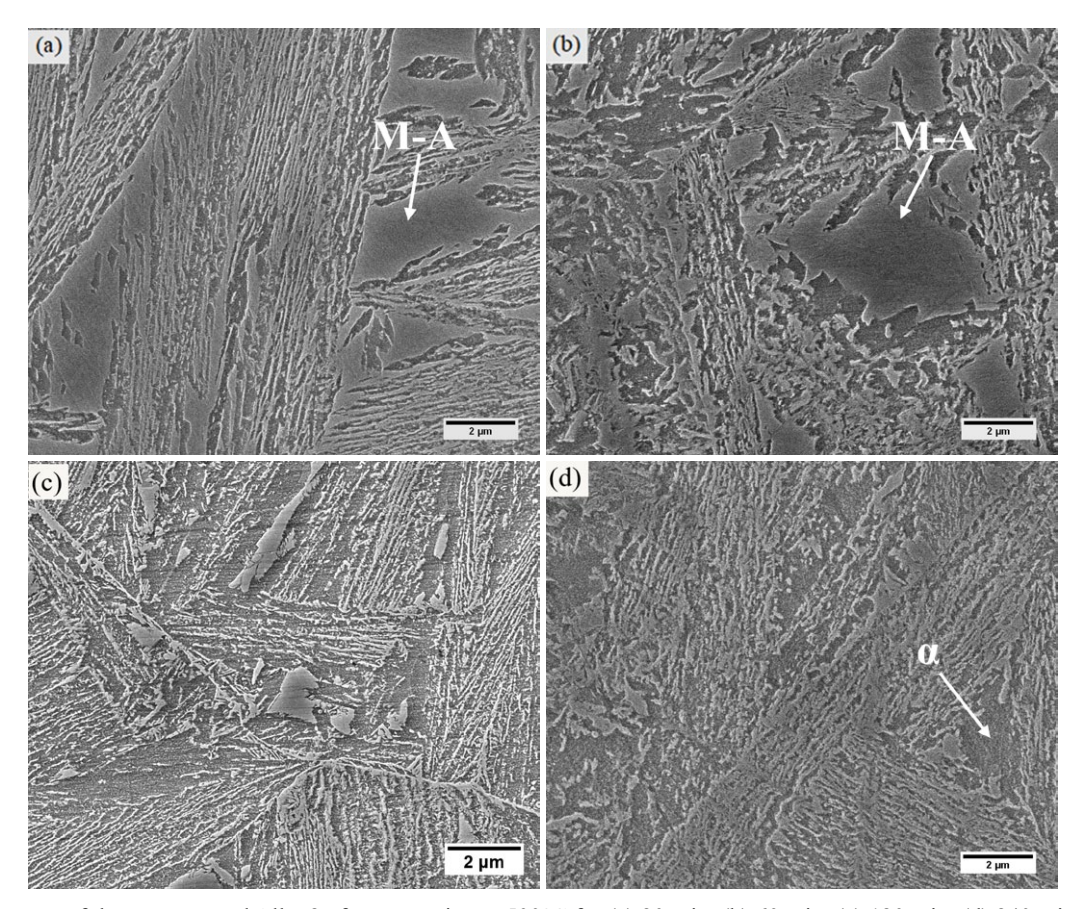


Fig. 16. SEM images of the austempered Alloy2 after tempering at 500°C for (a) 30 min, (b) 60 min, (c) 120 min, (d) 240 min. M: Martensite, M-A: Martensite-austenite constituents

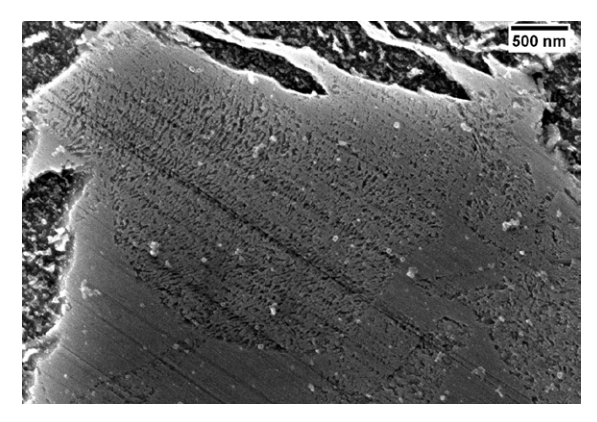


Fig. 17. SEM image of a M-A constituent of the austempered Alloy2 after tempering at 500°C for 30 min

The Peak Hardness Sample (450°C-2 h):

In the TEM images of the peak hardness sample, cementite precipitates are observed inside (Figs. 18a,b) and at the boundaries of the BF films (Fig. 18a). Indexing of the SAED (Selected Area Diffraction) pattern in Fig. 18b was performed by determining the radii (r_{hkl}) of the diffraction rings using ImageJ, calculating the interplanar spacing (d_{hkl}) values from the relation $r_{hkl} = 1/d_{hkl}$, and comparing the calculated d_{hkl} values with those of the related ICSD (Inorganic Crystal Structure Database) cards. In addition, zone axes of the spot diffraction patterns were

determined using Crystbox® software. As a result, bcc ferrite (Z = [0 -1 2]), retained austenite (Z = [1 -2 0]) and cementite were detected in the microstructure.

In previous studies [22,30-31], at the peak hardness condition, copper precipitates were found to exist as clusters with a *bcc* structure. These clusters were coherent and spherical with an average diameter of 1-5 nm [22-23,29,35]. It was also found that coherent copper precipitates could not be detected by conventional TEM method due to poor diffraction contrast, which was attributed to the similarity of scattering factors and atomic radii of copper and iron [24-26,42-43]. In this study, coherent copper precipitates at the peak aged condition could not be detected by TEM imaging and SAED due to similar reasons.

The Overaged Sample (500°C-4 h):

In Fig. 19a, cementite precipitates are seen at the ferrite boundaries and inside the ferrite films. The cementite precipitates assume spherical, ellipsoidal, and rod-like morphologies. A comparison of the microstructures of the overaged (Fig. 19a) and peak aged (Fig. 18) samples indicates that the cementite precipitates at the ferrite film boundaries have grown significantly faster than those inside the ferrite films, most likely due to faster diffusion kinetics at the boundaries.

As a result of indexing of the SAED pattern in Fig. 19c, cementite ($Z = [-4 \ 1 \ 3]$), bcc ferrite ($Z = [-1 \ 4 \ 6]$) and fcc copper were detected in the microstructure. In TEM images, copper

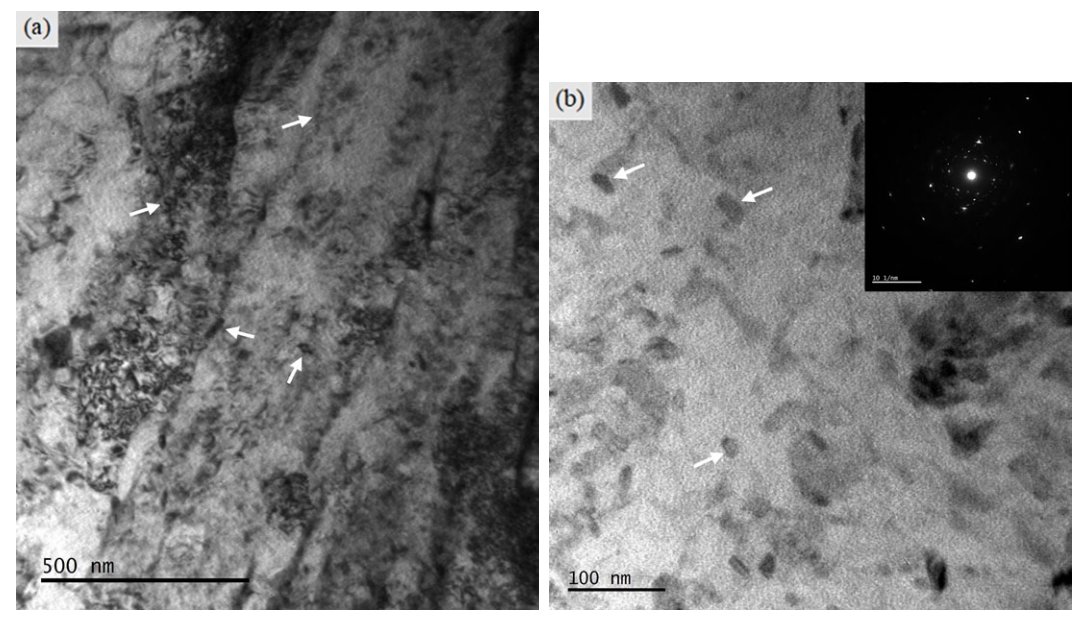


Fig. 18. Bright field TEM images (a,b) of the peak hardness sample at 450°C. Arrows: Cementite precipitates. Right top corner in (b): The SAED pattern

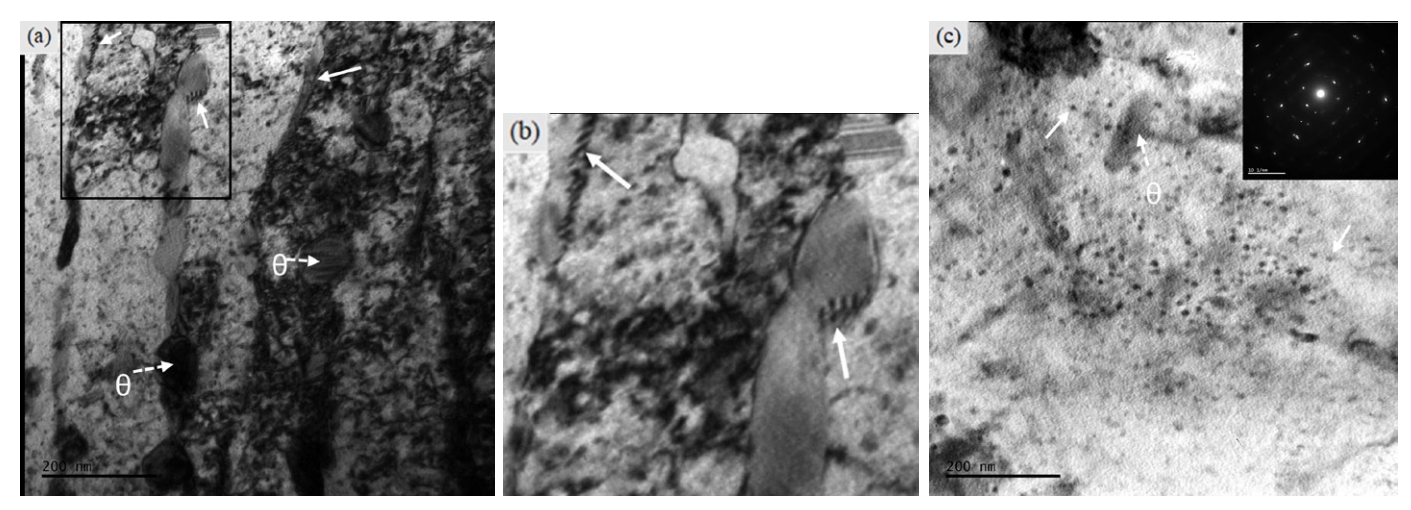


Fig. 19. Bright field TEM images (a-c) of the overaged sample (500°C-4 h). Image (b): The enlarged view of the enclosed region in (a). Solid arrows: copper precipitates on cementite/ferrite boundaries. Right top corner in (b): The SAED pattern

precipitates are observed inside (Figs. 19a-c) the ferrite films and at the boundaries (Figs. 19a,b) of the coarse cementite precipitates. The copper precipitates in the ferrite matrix are spherical and ellipsoidal in shape, while those at the boundaries of the coarse cementite precipitates are ellipsoidal. The size of the copper precipitates in the ferrite matrix (Fig. 19c) was analyzed using ImageJ. It was found that the feret diameter of 72% of the precipitates was in the range of 8-11 nm. EDX analysis of the precipitates was not possible due to the highly magnetic structure of the steel.

In Fig. 18, fine cementite precipitates resulting from the decomposition of RA films have been observed at ferrite film boundaries. During the growth of these precipitates, copper is partitioned away [44-46] since it is almost insoluble in cementite [4,45,47]. Precipitation of the ejected copper possibly occurs via interphase precipitation [44,46,47] mechanism, since copper

precipitates at the cementite/ferrite boundaries exhibit a common orientation relationship with ferrite as shown in Figs. 19a,b.

3.3. Thermal Stability of the Alloys

The thermal stability of the alloys can be compared on the basis of the amount of austenite that remains undecomposed at the tempering temperature. On cooling from the tempering temperature to room temperature, the amount of RA amount does not remain constant if martensite is formed. Therefore, the RA amount data in Fig. 5 should be evaluated in conjunction with the information on the presence of martensite. In this study, it has been found that no direct evidence of martensite exists in the SEM images of Alloy1 (Figs. 13-14) tempered at 450-500°C for 30-240 min. However, in the microstructure of Alloy2 tempered

at 500°C for 30-120 min (Figs. 16-17), M-A constituents were determined in decreasing amounts with time. The hardness results (Fig. 8) also confirmed the presence of martensite under the same conditions. In the light of this information, evaluation of the XRD results (Fig. 5) indicate that Alloy2 is thermally more stable than Alloy1. This can be mainly explained by its lower driving force for cementite precipitation provided by (i) the presence of 2 wt.% copper, which is insoluble in cementite [4], and (ii) the presence of 1 wt.% Ni, which -as a powerful austenite stabilizer [11]- shifts the T_0 curve (Fig. 4) to the left, thereby reducing the carbon content of austenite during bainitic transformation.

3.4. The Effect of Microstructural Changes on Hardness

During tempering of NB steels, the fine microstructure consisting of very thin BF and RA films is progressively degraded. The degradation occurs mainly by the gradual decomposition of BF and RA into ferrite and cementite, and coarsening [20] of the ferrite films. Decomposition of RA results in the formation of fine cementite precipitates at bainitic ferrite/RA boundaries (Fig. 17). These precipitates have been shown to slow down the coarsening of BF films [15]. When the increase in the ferrite film thickness becomes significant, hardness decreases considerably [15].

In NB steels which do not contain sufficient amounts of secondary/precipitation hardening [9,20,48] elements, hardness decreases [48] with time during tempering at temperatures that cause microstructural degradation, provided that martensite does not form on cooling to room temperature. This behavior was observed also in Alloy1. On the other hand, Alloy 2, which contains 2 wt.%Cu, yielded secondary hardening peaks in the range of 400-500°C. The secondary hardening peaks were attributed to the precipitation of copper, since these peaks were observed even under the tempering conditions (400-450°C) which did not result in the formation of martensite on cooling. The formation of martensite, which occurred on cooling from 500°C after tempering for 30 min, resulted in an ~5% higher peak hardness value as compared to those observed after tempering at 400-450°C (Fig. 7).

In the case of tempering of AT Alloy2, effects of copper on hardness can be summarized as follows:

- Copper precipitates increase hardness via pinning of dislocations [49]. Peak hardness is achieved when Cu precipitates (1-5 nm) [22-23,29,35] exist as coherent clusters with a *bcc* structure [22,30-31]. As tempering proceeds, coherency is reduced and finally lost, while crystal structure changes accordingly to 9R, 3R/detwinned 9R [50]/twinned fcc [32,51] and finally to fcc [22-23,27-29,35], respectively. With the reduction in coherency, a decrease in hardness is observed.
- Copper and cementite [15] precipitates at ferrite/RA boundaries (Fig. 18) slow down the coarsening of ferrite films via pinning effect.

• Copper, as a cementite inhibitor [4], in solid solution delays RA decomposition (Fig. 5).

4. Conclusion

In this study, the tempering response of two nanostructured bainitic steels of composition Fe-1C-2Si (wt.%) (Alloy1) and Fe-1C-2Si-2Cu-2Ni (wt.%) (Alloy2) was investigated. Main findings of the study are summarized as follows:

- Alloy 2 is thermally more stable than Alloy 1, which can be related to the lower driving force for cementite precipitation due to the presence of Cu and Ni.
- The bainitic samples of Alloy2 exhibit secondary hardening peaks when tempered at 400-500°C. However, the hardness of Alloy1 shows a decreasing trend under the same conditions.
- During tempering, the change in the hardness of Alloy1 is governed only by the degree of microstructural degradation, whereas that of Alloy2 is a result of the opposing effects of softening due to progressive microstructural degradation and hardening due to copper precipitation.
- Tempering of the SQ samples of Alloy2 results in the retardation of softening, which can be attributed to the copper precipitates. AT samples of Alloy2 exhibit higher hardness values than the SQ samples after tempering at 500°C for 30 in-120 min due to the formation of martensite on cooling to room temperature.
- TEM investigations of Alloy2 tempered at 500°C for 240 min showed that fcc copper precipitates exist inside the ferrite films and at the boundaries of the coarse cementite precipitates. Copper precipitates inside the ferrite matrix have a feret diameter in the range of 8-11 nm. Copper precipitates at the boundaries of coarse cementite precipitates are formed possibly during the growth of cementite by interphase precipitation mechanism, since a common orientation relationship with the ferrite matrix was observed.

Acknowledgements

The authors are grateful to Dr. Özgür Duygulu from TUBITAK Marmara Research Center for preparation and imaging of TEM samples, to Çemtaş Çelik Makina Sanayi ve Ticaret A.Ş. for JMatPro® calculations, and to Dr. Tolga Ertürk from Welding Technology & Non-destructive Testing Research/Application Center in Middle East Technical University for hardness measurements.

REFERENCES

[1] C. Garcia-Mateo, F.G. Caballero, Design of Carbide-free Low-temperature Ultra High Strength Bainitic Steels. Int. J. Mat. Res. **98** (2), 137-143 (2007).

DOI: https://doi.org/10.3139/146.101440

- [2] L. Morales-Rivas, H.-W. Yen, B.-M. Huang, M. Kuntz, F.G. Ca-ballero, J.-R. Yang, C. Garcia-Mateo, Tensile Response of Two Nanoscale Bainite Composite-Like Structures. JOM 67, 2223-2235 (2015). DOI: https://doi.org/10.1007/s11837-015-1562-x
- [3] H.K.D.H. Bhadeshia, Bainite in Steels: Theory and Practice, 3rd edn., Leeds 2015.
- [4] C. Hulme-Smith, The Thermal Stability of Bulk Nanocrystalline Steels. Ph.D. Thesis, University of Cambridge, 2016.
- [5] A. Kumar, A. Singh, Mechanical Properties Of Nanostructured Bainitic Steels. Materialia 15, 101034 (2021).
 DOI: https://doi.org/10.1016/j.mtla.2021.101034
- [61] C. Garcia-Mateo, F.G. Caballero, T. Sourmail, M. Kuntz, J. Cornide, V. Smanio, R. Elvira, Tensile Behaviour of a Nanocrystalline Bainitic Steel Containing 3 wt.% Silicon. Mater. Sci. Eng. A 549, 185-192 (2012).
 - DOI: https://doi.org/10.1016/j.msea.2012.04.031
- [7] M.N. Yoozbashi, T. Hajilou, E. Akbarzadeh Chiniforush, S. Yazdani, Mechanical Stability of Retained Austenite in the Nanostructured, Carbide Free Bainitic Steels during Tensile Testing and Cold Rolling Process. Int. J. ISSI 14 (2), 27-32 (2017).
- [8] M.A. Santajuana, R. Rementeria, M. Kuntz, J. Jimenez, F.G. Caballero, C. Garcia-Mateo, Low-Temperature Bainite: A Thermal Stability Study. Metall. Trans. A 49, 2026-2036 (2018).
 DOI: https://doi.org/10.1007/s11661-018-4595-2
- [9] V. Ruiz-Jimenez, M. Kuntz, T. Sourmail, F.G. Caballero, J.A. Jimenez, C. Garcia-Mateo, Retained Austenite Destabilization during Tempering of Low-Temperature Bainite. Appl. Sci. 10 (24), 8901 (2020). DOI: https://doi.org/10.3390/app10248901
- [10] A. Królicka, F.G. Caballero, W. Zalecki, R. Kuziak, R. Rozmus, Controlling the Thermal Stability of a Bainitic Structure by Alloy Design and Isothermal Heat Treatment. Materials 16 (8), 2963 (2023). DOI: https://doi.org/10.3390/ma16082963
- [11] C.N. Hulme-Smith, S.W. Ooi, H.K.D.H. Bhadeshia, Thermally Stable Nanocrystalline Steel. Metall. Trans. A 48, 4957-4964 (2017). DOI: https://doi.org/10.1007/s11661-017-4248-x
- [12] F.G. Caballero, M.K. Miller, C. Garcia-Mateo, Atom Probe Tomography Analysis of Precipitation during Tempering of a Nanostructured Bainitic Steel. Met. Mat. Trans. A 42, 3660-3668 (2011). DOI: http://dx.doi.org/10.1007/s11661-011-0699-7
- [13] M.J. Peet, S.S. Babu, M.K. Miller, H.K.D.H. Bhadeshia, Tempering of Low-Temperature Bainite. Met. Mat. Trans. A 48, 3410-3418 (2017).
 DOI: https://doi.org/10.1007/s11661-017-4086-x
- [14] C.N. Hulme-Smith, I. Lonardelli, M.J. Peet, A.C. Dippel, H.K.D.H. Bhadeshia, Enhanced Thermal Stability in Nanostructured Bainitic Steel. Scr. Mater. 69 (2), 191-194 (2013). DOI: https://doi.org/10.1016/j.scriptamat.2013.03.029
- [15] C. Garcia-Mateo, M. Peet, F.G. Caballero, H.K.D.H. Bhadeshia, Tempering of Hard Mixture of Bainitic Ferrite and Austenite. Mater. Sci. Technol. 20 (7), 814-818 (2004). DOI: https://doi.org/10.1179/026708304225017355
- [16] A. Krolicka, A.M Zak, F.G. Caballero, Enhancing Technological Prospect of Nanostructured Bainitic Steels by the Control of Thermal Stability of Austenite. Mater. Des. 211, 110143 (2021). DOI: https://doi.org/10.1016/j.matdes.2021.110143

- [17] C. Garcia-Mateo, F.G. Caballero, H.K.D.H. Bhadeshia, Development of Hard Bainite. ISIJ Int. 43 (8), 1238-1243 (2003).
 DOI: https://doi.org/10.2355/isijinternational.43.1238
- [18] I. Pushkareva, B. Shalchi-Amirkhiz, S.Y.P. Allain, G. Geandier, F. Fazeli, M. Sztanko, C. Scott, The Influence of Vanadium Additions on Isothermally Formed Bainite Microstructures in Medium Carbon Steels Containing Retained Austenite. Metals 10 (3), 392 (2020). DOI: https://doi.org/10.3390/met10030392
- [19] C.N. Hulme-Smith, S.W. Ooi, H.K.D.H. Bhadeshia, Intermetallic-strengthened Nanocrystalline Bainitic Steel. Mater. Sci. Technol. 34 (16), 1976-1979 (2018).
 DOI: https://doi.org/10.1080/02670836.2018.1501145
- [20] A. Królicka, F.G. Caballero, R. Kuziak, K. Radwański, L. So-zańska-Jędrasik, P. Stawarczyk, Two Design Strategies for Enhancing the Thermal Stability of Bainitic Structures. J. Mater. Res. Technol. 24, 7004-7020 (2023).
 DOI: https://doi.org/10.1016/j.jmrt.2023.05.003
- [21] X. Shen, D. Görzen, Z. Xu, B. Blinn, W. Bleck, T. Beck, U. Krupp, W. Song, Nano-sized Cu Precipitation and Microstructural Evolution in Aged Ultralow and Medium Carbon Steels. Materialia 26, 101626 (2022). DOI: https://doi.org/10.1016/j.mtla.2022.101626
- [22] M.S. Gagliano, M.E. Fine, Characterization of the Nucleation and Growth Behavior of Copper Precipitates in Low-Carbon Steels. Metall. Trans. A 35, 2323-2329 (2004). DOI: https://doi.org/10.1007/s11661-006-0212-x
- [23] N. Maruyama, M. Sugiyama, T. Hara, H. Tamehiro, Precipitation and Phase Transformation of Copper Particles in Low Alloy Ferritic and Martensitic Steels. Mater. Trans. JIM 40 (4), 268-277 (1999). DOI: https://doi.org/10.2320/matertrans1989.40.268
- [24] M.P. Phaniraj, YM. Shin, WS Jung, MH Kim, IS Choi, Understanding Dual Precipitation Strengthening in Ultra-High Strength Low Carbon Steel Containing Nano-Sized Copper Precipitates and Carbides. Nano Converg. 4, 16 (2017). DOI: https://doi.org/10.1186/s40580-017-0110-5
- [25] C.S. Pande, M.A. Imam, Nucleation and Growth Kinetics in High Strength Low Carbon Ferrous Alloys. Mater. Sci. Eng. A 457 (1-2), 69-76 (2007). DOI: https://doi.org/10.1016/j.msea.2006.12.043
- [26] S.R. Goodman, S.S. Brenner, J.R. Low, An FIM-Atom Probe Study of the Precipitation of Copper From Iron-1.4 at. pct Copper. Part I: Field-Ion Microscopy. Metall. Trans. 4, 2363-2369 (1973). DOI: https://doi.org/10.1007/BF02669376
- [27] O.E. Uzer, The Aging Characteristics of a Medium Carbon Steel with and without Copper. M.Sc. Thesis, Middle East Technical University, Ankara (2019).
- [28] R. Monzen, M.L. Jenkins, A.P. Sutton, The bcc-to-9R Martensitic Transformation of Cu Precipitates and the Relaxation Process of Elastic Strains in an Fe-Cu Alloy. Philos. Mag. A 80 (3), 711-723 (2000). DOI: https://doi.org/10.1080/01418610008212077
- [29] P.J. Othen, M.L. Jenkins, G.D.W. Smith, W.J. Phytian, Transmission Electron Microscope Investigations of the Structure of Copper Precipitates in Thermally-aged Fe–Cu and Fe–Cu–Ni. Philos. Mag. Lett. 64 (6), 383-391 (1991).
 DOI: https://doi.org/10.1080/09500839108215121

- [30] P.J. Othen, M.L. Jenkins, G.D.W. Smith, High-Resolution Electron Microscopy Studies of The Structure of Cu Precipitates in α-Fe. Philos. Mag. A 70 (1), 1-24 (1994).
 DOI: https://doi.org/10.1080/01418619408242533
- [31] S. Pizzini, K.J. Roberts, W.J. Phythian, C.A. English, G.N. Greaves, A Fluorescence EXAFS Study of the Structure of Copperrich Precipitates in Fe–Cu and Fe–Cu–Ni Alloys. Philos. Mag. Lett. 61 (4), 223-229 (1990).
 DOI: https://doi.org/10.1080/09500839008202362
- [32] F. Maury, N. Lorenzelli, M.H. Mathon, C.H. de Novion, P. Lagarde, Copper Precipitation in FeCu, FeCuMn, and FeCuNi Dilute Alloys followed by X-ray Absorption Spectroscopy. J.Phys.-Condens. Matter 6 (2), 569 (1997).
 DOI: https://dx.doi.org/10.1088/0953-8984/6/2/027
- [33] Y.-U. Heo, Y.-K. Kim, J.-S. Kim, J.-K. Kim, Phase Transformation of Cu Precipitates from bcc to fcc in Fe–3Si–2Cu Alloy. Acta Mater. 61 (2), 519-528 (2013).
 DOI: https://doi.org/10.1016/j.actamat.2012.09.068
- [34] S.R. Goodman, S.S. Brenner, J.R. Low, An FIM-atom Probe Study of the Precipitation of Copper from Iron-1.4 at. pct Copper. Part II: Atom Probe Analyses. Metall. Trans. 4, 2371-2378 (1973). DOI: https://doi.org/10.1007/bf02669377
- [35] O.N. Mohanty, Forging Grade Steels for Automotives. In: R. Rana, S.B. Singh (Ed.), Automotive Steels: Design, Metallurgy, Processing and Applications, Woodhead Publishing (2017).
- [36] H. Huang, M.Y. Sherif, P.E.J. Rivera-Díaz-del-Castillo, Combinatorial Optimization of Carbide-free Bainitic Nanostructures. Acta Mater. 61 (5), 1639-1647 (2013).
 DOI: https://doi.org/10.1016/j.actamat.2012.11.040
- [37] F.G. Caballero, M.J. Santofimia, C. Capdevila, C. Garcia-Mateo, C. Garcia-de-Andres, Design of Advanced Bainitic Steels by Optimisation of TTT Diagrams and T₀ Curves. ISIJ Int. 46 (10), 1479-1488 (2006). DOI: https://doi.org/10.2355/isijinternational.46.1479
- [38] https://www.phase-trans.msm.cam.ac.uk/map/steel/programs/mucg83.html
- [39] F.G. Caballero, M.K. Miller, C. Garcia-Mateo, C. Capdevila, S.S. Babu, Redistribution of Alloying Elements during Tempering of a Nanocrystalline Steel. Acta Mater. 56 (2), 188-199 (2008). DOI: https://doi.org/10.1016/j.actamat.2007.09.018
- [40] J. Zhu, G. Barber, X. Sun, Effects of Isothermal Temperature on Dislocation Density in Bainite Transformation of 4140 Steel. Materials 15 (17), 6066 (2022).
 DOI: https://doi.org/10.3390/ma15176066

- [41] G.K. Williamson, W.H. Hall, X-ray Line Broadening from Filed Aluminium and Wolfram. Acta Metall. 1 (1), 22-31 (1953). DOI: https://doi.org/10.1016/0001-6160(53)90006-6
- [42] A. Youle, B. Ralph, A Study of the Precipitation of Copper from α-Iron in the Pre-Peak to Peak Hardness Range of Ageing. Met. Sci. J. 6 (1), 149-152 (1972). DOI: https://doi.org/10.1179/030634572790446253
- [43] E. Hornbogen, The Role of Strain Energy during Precipitation of Copper and Gold from Alpha Iron. Acta Metall. **10** (5), 525-533 (1962). DOI: https://doi.org/10.1016/0001-6160(62)90197-9
- [44] J.A. Wasynczuk, R.M. Fisher, G. Thomas, Effects of Copper on Proeutectoid Cementite Precipitation. Metall. Trans. A 17, 2163-2173 (1986). DOI: https://doi.org/10.1007/bf02645914
- [45] J.A. Wasynczuk, Precipitation of Proeutectoid Cementite, Pearlite, and Epsilon-Copper in Iron-Carbon-Copper Alloys (Steel, Phase-Transformations). Ph.D. Thesis, University of California, Berkeley (1986).
- [46] T. Chairuangsri, D.V. Edmonds, The Precipitation of Copper in Abnormal Ferrite and Pearlite in Hyper-eutectoid Steels. Acta Mater. 48 (15), 3931-3949 (2000). DOI: https://doi.org/10.1016/S1359-6454(00)00176-2
- [47] G. Fourlaris, A.J. Baker, G.D. Papadimitriou, Microscopic Characterisation of ε-Cu Interphase Precipitation in Hypereutectoid Fe-C-Cu Alloys. Acta Metall. Mater. **43** (7), 2589-2604 (1995). DOI: https://doi.org/10.1016/0956-7151(94)00474-V
- [48] G. Kafadar, A. Kalkanli, A.T. Özdemir, B. Ögel, Effect of Isothermal Transformation Treatment and Tempering on the Microstructure and Hardness of a Medium C and High Si Steels. ISIJ Int. 61 (5), 1679-1687 (2021).
 DOI: https://doi.org/10.2355/isijinternational.isijint-2020-419
- [49] H. Sun, D. Li, Y. Diao, Y. He, L. Yan, X. Pang, K. Gao, Nanoscale Cu Particle Evolution and its Impact on the Mechanical Properties and Strengthening Mechanism in Precipitation-hardening Stainless Steel. Mater. Charact. 188, 111885 (2022). DOI: https://doi.org/10.1016/j.matchar.2022.111885
- [50] G. Han, Z.J. Xie, Z.Y. Li, B. Lei, C.J. Shang, R.D.K. Misra, Evolution of Crystal Structure of Cu Precipitates in a Low Carbon Steel. Mater. Des. 135, 92-101 (2017).
 DOI: https://doi.org/10.1016/j.matdes.2017.08.054
- [51] R. Nizinkovskyi, T. Halle, M. Krüger, Influence of Elasticity on the Morphology of fcc-Cu Precipitates in Fe-Cu Alloys. A Phasefield Study. J. Nucl. Mater. 566, 153764 (2022). DOI: https://doi.org/10.1016/j.jnucmat.2022.153764